JOURNAL OF MATERIALS SCIENCE 35 (2000) 4885–4893

1 : 2 Long-range ordering and defect mechanism of WO_3-doped perovskite $Ba(Mg_{1/3}Ta_{2/3})O_3$

YOUNG K. KIM, KYU-MANN LEE, HYUN M. JANG*
Department of Materials Science and Engineering, and Laboratory for Physics/Chemistry of Dielectric Materials, Pohang University of Science and Technology (POSTECH), Pohang 790-784, South Korea
E-mail: hmjang@postech.ac.kr

The nature of the B-site cation ordering and the associated defect process necessary to stabilize the ordered domains were investigated using the WO_3-doped $Ba(Mg_{1/3}Ta_{2/3})O_3$ (BMT) system as a typical example of $Ba(B'_{1/3}B''_{2/3})O_3$-type complex perovskites. It was shown that only the 1 : 2 long-range ordering of the B-site cation existed in both undoped and WO_3-doped BMT perovskites. The atomic defect mechanism associated with the stoichiometric 1 : 2 long-range ordering was systematically investigated. It is concluded that the substitution of W^{6+} for Ta^{5+} in the WO_3-doped BMT enhances the degree of the 1 : 2 long-range ordering and produces the positively charged $W^{\bullet}_{Ta}$ sites with a concomitant generation of tantalum vacancies (V''''''_{Ta}) and mobile oxygen vacancies ($V^{\bullet\bullet}_{O}$) for the ionic charge compensation. © *2000 Kluwer Academic Publishers*

1. Introduction

Microwave technology has made a remarkable progress, along with the recent development of advanced communication systems. In particular, dielectric resonator has achieved an important position as the key element in microwave integrated circuits and in microwave filters. Microwave devices are required to have small size, high-level temperature stability, and low power loss [1–3]. Therefore, dielectric materials for the resonators should possess high dielectric permittivities, small temperature coefficients of resonant frequency (TCF $\leq \pm 10$ ppm/°C), and high unloaded quality factors (Q factor) for a stable resonant frequency. Among these, the unloaded quality factor is the most important property for the development of low noise oscillators and narrow band microwave filters with low insertion losses. Since the unloaded quality factor is only limited by the material's quality factor ($Q = 1/\tan\delta$) [4], the dielectric loss is the determining property for the behavior of dielectric resonators. It is known that the dielectric loss at microwave frequencies is usually caused by the lattice anharmonic interaction [5], by the disordered charge distribution for nonconducting ionic crystals [6], and by the lattice imperfections (e.g., impurities, dislocations, local strains, etc.) [7].

$Ba(Mg_{1/3}Ta_{2/3})O_3$ (referred to as BMT) is one of the most extensively studied $Ba(B'_{1/3}B''_{2/3})O_3$-type complex perovskites and has the highest quality factor among microwave dielectric ceramics. This material is characterized by large dielectric permittivity (~25 at 10 GHz), small TCF (~0 ppm/°C), and high unloaded Q factor ($Q \times f \sim 170{,}000$) [8]. It is known that the B-site cation ordering has a large influence on the dielectric loss at microwave frequencies in BMT or, more generally, in $Ba(B'_{1/3}B''_{2/3})O_3$-type complex perovskites [8]. The most efficient way of reducing the dielectric loss at microwave frequency range is the formation of the stoichiometric 1 : 2 long-range ordered clusters [8, 9]. However, due to low sinterability, the sintering at an elevated temperature (~1650°C) and the subsequent long-time annealing are required for the fabrication of BMT [8, 10, 11]. In order to overcome this problem, various additives with their melting points lower than BMT were investigated, and their effects on dielectric properties were examined [8, 12]. Yoon and co-workers [13] reported that the addition of $BaWO_4$ and the subsequent sintering at temperatures above 1430°C increased the unloaded Q factor of BMT.

They attributed the observed increase in the unloaded Q factor to (i) the enhancement of the B-site cation ordering and (ii) the elimination of oxygen vacancies by the substitution of W^{6+} ions for Ta^{5+} ions in the B-site sublattice of the perovskite BMT [13]. The positively charged $W^{\bullet}_{Ta}$ sites produced by the substitution then increase the differences in the charge and the ionic radius between the B-site ions and, thus, promote the ordering tendency of the B-site cations. According to Yoon and co-workers [13], the elimination of oxygen vacancies upon the substitution of W^{6+} ions for Ta^{5+} ions can be represented by the following defect equation:

$$\begin{gathered} 2WO_3 \overset{Ta_2O_5}{\longleftrightarrow} 2W^{\bullet}_{Ta} + 5O_O + 1/2O_2 + 2e' \\ 1/2O_2 + V^{\bullet\bullet}_{O} + 2e' \leftrightarrow O_O \\ \hline 2WO_3 + V^{\bullet\bullet}_{O} \overset{Ta_2O_5}{\longleftrightarrow} 2W^{\bullet}_{Ta} + 6O_O \end{gathered} \quad (1)$$

* Author to whom all correspondence should be addressed.

However, one does expect that the stoichiometric 1 : 2 ordered regions become unstable by the substitution because the excess charges ($W_{Ta}^{\bullet}$) are generated within the neutrally ordered regions. Consequently, the ordering tendency should be decreased by the substitution of W^{6+} ions. Contrary to this expectation, the B-site cation ordering was enhanced by the addition of $BaWO_4$ [13].

This contradictory observation suggests the possibility of the occurrence of the following types of processes upon the substitution of W^{6+} ion for Ta^{5+} ion: (i) a new type of the B-site cation ordering other than the stoichiometric 1 : 2 ordering, and (ii) a defect chemical mechanism other than the process described in Equation 1 for the stabilization of the ordered regions. Therefore, one should seek the possibility of the occurrence of these processes (or one of these) to clearly understand the controlling mechanism of the enhanced ordering in the WO_3-doped BMT perovskite. For this purpose, it is necessary to systematically examine the dissolution behavior of the excess added WO_3 dopant in the perovskite structure and the atomic defect mechanism directly related to the enhanced B-site cation ordering.

In view of these facts, the main purpose of the present study is to clearly identify the atomic defect mechanism that leads to the enhanced B-site ordering in the WO_3-doped BMT. For this purpose, we examined the nature of the B-site ordering in both undoped and WO_3-doped BMT's first. Then, the dissolution behavior of the excess added WO_3 was investigated by examining the Rietveld patterns. Based on this information, the main atomic defect process (i.e., charge compensation mechanism) associated with the 1 : 2 ordering was identified by systematically examining the electrical conductivity as a function of the partial pressure of oxygen and temperature.

2. Experimental procedure

The composition of the WO_3-doped BMT system used in this study is in the range of 0 to 6 mol % of WO_3 and can be represented by BMT-$x$$WO_3$ with $0 \leq x \leq 0.06$. In the preparation of the WO_3-doped BMT, stoichiometric amounts of analytical reagent (AR) grade $BaCO_3$, MgO, and Ta_2O_5 were ball-milled in alcohol with ZrO_2 media for 16 h. If necessary, an appropriate amount of WO_3 was also added to the mixture. The dried powder was calcined at 1250°C for 4 h.

After the calcination, an additional ball-milling step was added to ensure a fine particle size before sintering. The dried powders were first pressed as disks and then cold-isostatically pressed under 190 MPa pressure. The pressed pellets were sintered at 1600°C for 4 h with a heating/cooling rate of 5°C/min.

XRD (Rigaku, DMAX-3B, Japan) patterns of the heat-treated samples were recorded over the angular range of $10^\circ \leq 2\theta \leq 80^\circ$ by steps of 0.04°. The instrumental aberrations were corrected by the external standard method with standard Si powders (NBS, SRM 640b, USA). The structure refinements using the Rietveld method (program: Rietan [14]) were carried out to determine the change of crystal structure with the excess WO_3. The lattice parameters were calculated from XRD data using the least square program for a Rigaku DMAX-B diffractometer.

The degree of the long-range ordering was quantitatively determined by the value of the Mg-site occupancy of Mg atoms obtained using the Rietveld analysis of XRD data. The degree of long-range ordering (S) can formally be written as

$$S = \frac{Mg_{Mg} - Mg_{Mg}(dis.)}{Mg_{Mg}(ord.) - Mg_{Mg}(dis.)} \quad (2)$$

where Mg_{Mg}(dis.) and Mg_{Mg}(ord.) are the Mg-site occupancy of Mg atoms in a fully disordered state and in a fully ordered state, respectively. In case of BMT, Mg_{Mg}(dis.) is $1/3$ and Mg_{Mg}(ord.) is 1.

Samples for the electrical conductivity measurements were coated with platinum-based electrode and heat-treated at 1000°C for 1 h. The DC conductivity values of the BMT specimens at various temperatures were measured with a picoammeter/voltage source (Model 487, Keithley, Inc.) for a measuring voltage between $+5$ and -5 V. The resistance values were recorded after a fixed waiting period (typically 30 min). Temperature was measured using a Keithley 740 thermometer via a R-type thermocouple. For the measurement of electrical conductivity as a function of the oxygen partial pressure, a mixture of O_2 and Ar was flowed. UHC 1500A mass flow controllers (MFC) were used to control the partial pressure of oxygen. In order to read a correct partial pressure, a zirconia oxygen sensor was used.

Samples for transmission electron microscopy (TEM) were mechanically polished to 100 μm and dimpled from both sides to obtain a thickness of about 15 μm at the center. Suitable TEM specimens were finally obtained by ion beam thinning, using argon ions at 4 kV and an incident angle of 15° to the specimen. Microscopic examination was carried out using a transmission electron microscope (Philips-CM 30) operated at 300 kV.

X-ray photoelectron spectroscopy (XPS; Perkin Elmer, PHI 5000 ESCA, USA) profiles of the heat-treated samples were obtained using an Mg K_α source (1253.6 eV) with a linewidth of 0.7 eV. The samples were maintained at 298 K under a vacuum level of below 2×10^{-9} torr during the analysis. The C_{1S} peak (285.0 eV) was used as the reference standard [15].

3. Results and discussion

3.1. The nature of B-site cation ordering

It is known that $A(B'_{1/3}B''_{2/3})O_3$-type complex perovskites can undergo two different types of the B-site cation ordering. One is the nonstoichiometric 1 : 1 short-range ordering, and the other is the stoichiometric 1 : 2 long-range ordering [9]. Although it is reported that the stoichiometric 1 : 2 ordering dominates over the nonstoichiometric 1 : 1 ordering in $Ba(B'_{1/3}B''_{2/3})O_3$-based systems [16], the exact nature of the B-site cation ordering is not well-known for BMT-based systems. On the other hand, the nonstoichiometric 1 : 1 short-range ordering predominates over the 1 : 2 long-range ordering in $Pb(B'_{1/3}B''_{2/3})O_3$-based systems [9, 17, 18].

If the Mg/Ta ratio within an ordered domain of the BMT-based systems is 1 : 2, any charge imbalance and compositional partitioning between the ordered domain and the disordered region will not be involved because this ratio coincides with the global Mg/Ta ratio. However, the substitution of W^{6+} ions for Ta^{5+} ions in the B-site sublattice of BMT would produce the charged ordered regions. In this case, there are two possible processes that compensate the excess charge caused by the formation of $W^{\bullet}_{Ta}$ sites. One is the formation of the nonstoichiometric 1 : 1 ordering rather than the stoichiometric 1 : 2 ordering. For the nonstoichiometric 1 : 1 ordering of $A(B'_{1/3}B''_{2/3})O_3$-type complex perovskites, the B′-rich ordered domain has a net negative charge with respect to the B″-rich disordered matrix region because the B′/B″ ratio is 1 : 1 within the ordered domain (as opposed to 1 : 2 for the average composition) [9, 17, 18]. However, the negatively charged ordered region can be compensated by the substitution of W^{6+} ions for Ta^{5+}. The other possibility of the charge compensation is the generation of some defects that compensates the positively charged $W^{\bullet}_{Ta}$ sites. Then, this would promote the stoichiometric 1 : 2 long-range ordering rather than the 1 : 1 ordering. Therefore, we have examined the nature of the B-site cation ordering first (i.e., 1 : 1 versus 1 : 2 ordering).

Fig. 1a presents the ⟨110⟩ zone-axis SADP (selected area diffraction pattern) of the pure, undoped BMT, showing $\{h \pm 1/3,\ k \pm 1/3,\ l \pm 1/3\}$ reflections. The presence of $\{h \pm 1/3,\ k \pm 1/3,\ l \pm 1/3\}$ reflections is caused by the stoichiometric 1 : 2 long-range ordering of the B-site cations (Mg^{2+} and Ta^{5+}) [9]. This gives rise to a hexagonal structure along the [001] directions [16]. Fig. 1b shows a centered dark-field image of the undoped BMT obtained using the (1/3 1/3 1/3) superlattice reflection, indicating the presence of the ordered microregions approximately a few hundreds nanometer in size. Fig. 1c is the ⟨110⟩ zone-axis SADP taken from the 2 mol% WO_3-doped BMT specimen, also exhibiting $\{h \pm 1/3, k \pm 1/3, l \pm 1/3\}$ superlattice reflections.

The TEM micrographic study clearly indicates that, regardless of the WO_3-doping, only the stoichiometric 1 : 2 long-range ordering exists in the BMT-based systems. From the results of TEM observations (Fig. 1), one can conclude that charged lattice defects (e.g., cation vacancies, oxygen vacancies, etc.) should be generated for the compensation of the excess charge of the ordered region formed by the substitution of W^{6+} ions for Ta^{5+} ions. However, a systematic analysis of the dissolution behavior of WO_3 and the ionic valence state of W ions in BMT should be preceded before one can clearly elucidate the atomic defect mechanism occurring in the WO_3-doped BMT system, and this is the subject of the next section.

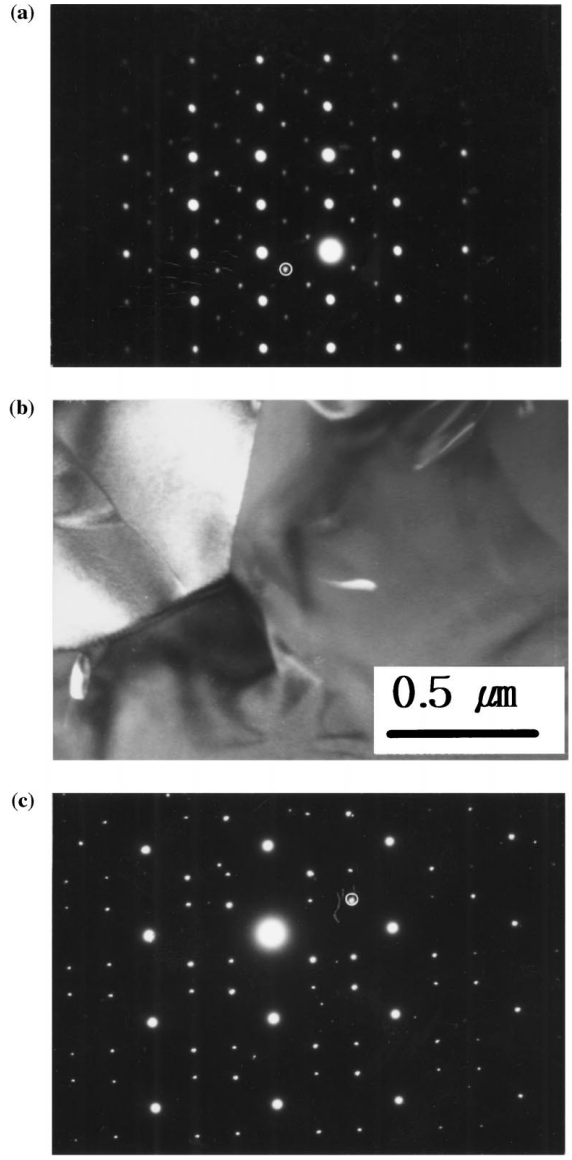

Figure 1 Transmission electron micrographs of BMT-$x$$WO_3$ specimens sintered at 1600°C for 4hrs: (a) SADP of undoped BMT specimen, (b) dark-field image of undoped BMT specimen obtained using (1/3 1/3 1/3) superlattice reflection, and (c) SADP of 2 mol % WO_3-doped BMT specimen.

3.2. Dissolution behavior of WO_3

3.2.1. Ionic valence state

Since tungsten (W) atom employed in the present study is a transition metal element, the valence state of W ions in a solid solution varies depending on chemical environments surrounding a given W ion. In this study, the ionic valence of W ions in the BMT-$x$$WO_3$ specimens was investigated using X-ray photoelectron spectroscopy (XPS). The XPS profiles of both the undoped BMT and the 6 mol % WO_3-doped BMT are shown in Fig. 2. Since the apparent binding energy of dielectric materials deduced from photoelectron spectrum is usually larger than the true binding energy [19], the C_{1s} spectrum has been used to evaluate the true binding energy. The difference between the apparent binding energy and the true binding energy of the undoped BMT is 4 ± 0.2 eV while that of the WO_3-doped BMT is 3.8 ± 0.2 eV.

As presented in the figure, $4f_{7/2}$, $4f_{5/2}$, and $5p_{3/2}$ photoelectron peaks of Ta are observed at the same binding energy for both the undoped BMT and the WO_3-doped BMT. This clearly indicates that the effective ionic valence of Ta ion is +5 and is not affected by the addition of WO_3. The photoelectron peak of 4f state of W in the WO_3-doped BMT is observed at 36 eV (Fig. 2), and

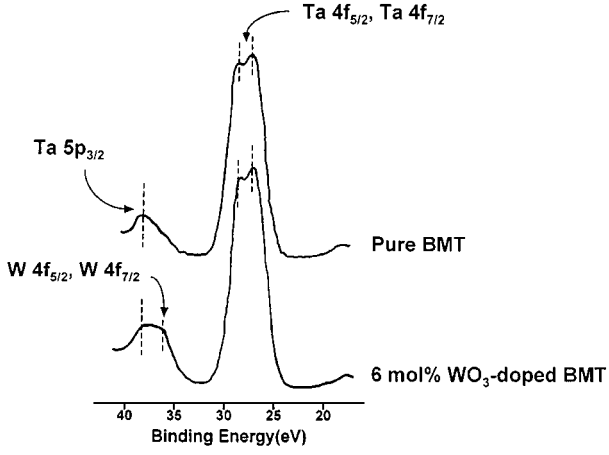

Figure 2 XPS profile of undoped (pure) and 6 mol % WO_3-doped BMT specimens.

this value is very close to the binding energy of 4f photoelectrons of W in WO_3 (i.e., 35.7 eV). On the other hand, the binding energy of 4f photoelectrons in WO_2 is 32.7 eV [20]. Therefore, one can conclude that W ion in the WO_3-doped BMT exists as a hexavalent state (W^{6+}).

3.2.2. Dissolution behavior and solubility limit

The dissolution behavior of WO_3 in the BMT-$x$$WO_3$ specimens was investigated by examining the Rietveld patterns. The Rietveld analysis [21] is actively used in the refinement of the structural parameters. The Rietveld refinement pattern of the 2 mol % WO_3-doped BMT is shown in Fig. 3. As shown in the figure, the observed XRD data are presented by the cross points and the calculated pattern is displayed by the solid line overlying them. The lower portions (ΔY) of the plot represent the difference between the observed and calculated intensities.

In the Rietveld analysis the parameters in a given structure model are adjusted in a computer simulation until the best fit of the least-square is obtained. For the elucidation of the substitution mechanism of W^{6+} ions in the BMT system, we have performed a computer simulation assuming that the added W^{6+} ions substitute for

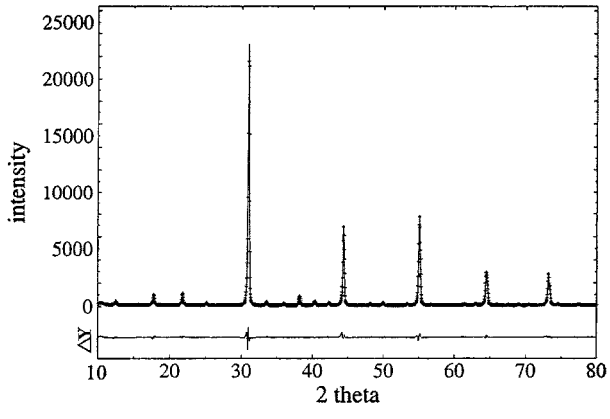

Figure 3 Rietveld refinement pattern of 2 mol % WO_3-doped BMT specimen.

TABLE I Reliability factors refined in the Rietveld analysis of 2 mol % WO_3-doped BMT specimen

	W^{6+} substituted for Ba-sites	W^{6+} substituted for Ta-sites	W^{6+} substituted for Ma-sites
R_{wp}	14.58	9.46	9.97
R_p	10.42	6.24	7.02
R_i	6.96	4.98	6.12

※ R_{wp} : weighted pattern R-factor.
R_p : pattern R-factor.
R_i : integrated intensity R-factor.

various sites in the perovskite sublattices. The final R factors for the 2 mol% WO_3-doped BMT specimen are listed in Table I. The definition of various R factors appeared in Table I is identical to that given by Young and Wiles [22]. As shown in Table I, the final R factors converge most satisfactorily when one assumes that W^{6+} ions substitute for Ta^{5+} ions in the B-site sublattice.

In addition to the R factors discussed above, the lattice parameter determined by the least square method decreases slightly with the amount of excess WO_3 (cubic lattice parameter; $a = 4.08836 \pm 0.000539$ Å for pure BMT versus $a = 4.08586 \pm 0.000843$ Å for 2 mol % WO_3-doped BMT), indicating that smaller ions substitute for larger ions in the perovskite BMT. Considering the effective ionic radius of the constituent ions [$W^{6+} = 0.58$ Å, $Ta^{5+} = 0.64$ Å, and $Mg^{2+} = 0.72$ Å] [23], one can expect that the observed slight decrease of the lattice parameter is caused by the substitution of W^{6+} ions for Ta^{5+} ions. Therefore, the analysis of XRD data indicates that the excess added W^{6+} ions substitute for Ta^{5+} ions in the B-site sublattice of the perovskite BMT.

Another evidence of the incorporation of excess WO_3 into the Ta-sites was obtained by examining the second phases formed above the solubility limit of WO_3. The X-ray diffraction patterns presented in Fig. 4 indicate the presence of the minority phases ($Ba_{0.5}TaO_3$ and $BaWO_4$) formed for the WO_3 content above 2 mol %. Contrary to this, the second phase is essentially absent for the WO_3-doping level below 2 mol %, indicating that the solubility limit of WO_3 in the perovskite BMT is

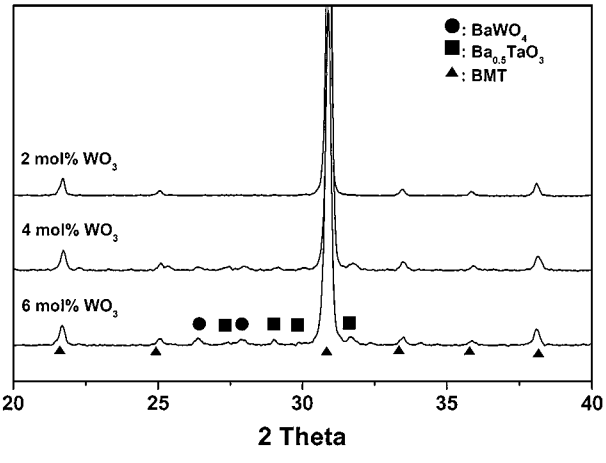

Figure 4 XRD patterns of BMT-$x$$WO_3$ specimens containing various amounts of excess WO_3.

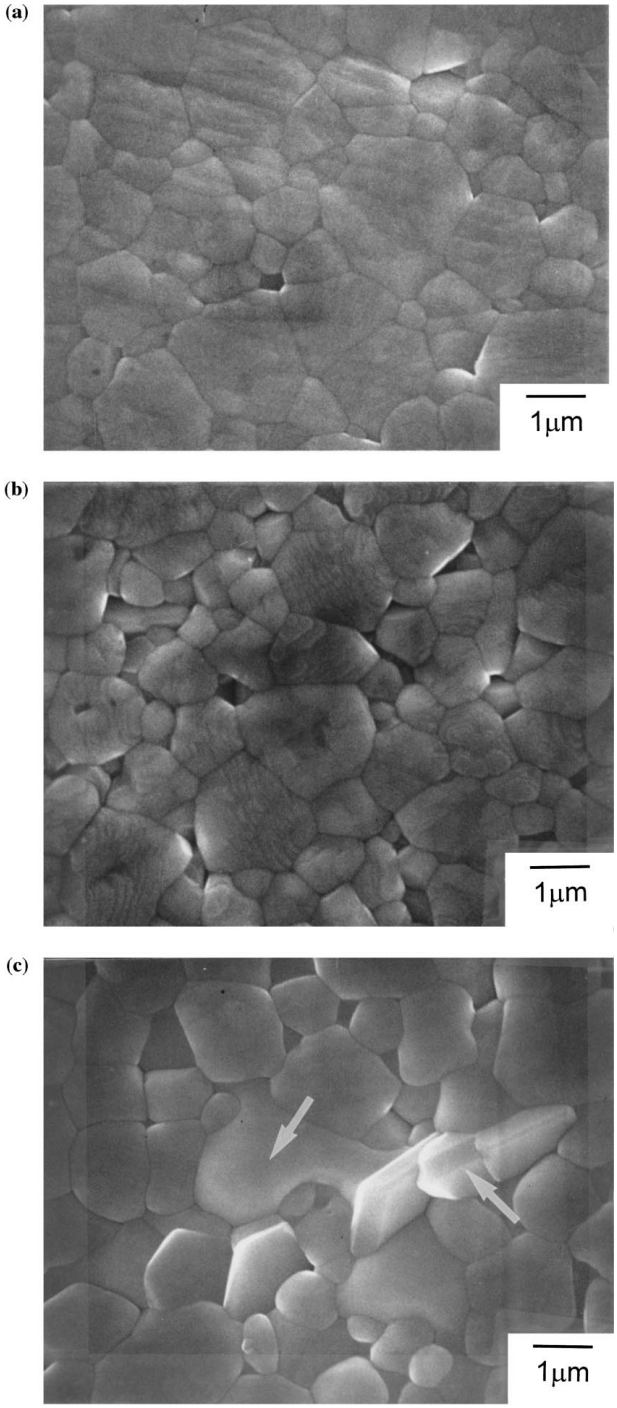

Figure 5 Scanning electron micrographs of sintered BMT-$x$$WO_3$ after thermal etching at 1300°C for 1 hr: (a) $x = 0.00$, (b) $x = 0.02$, and (c) $x = 0.06$.

~2 mol %. In addition to this, we have observed that the content of $Ba_{0.5}TaO_3$ phase increases with the amount of excess WO_3. This observation further supports the previous conclusion that the added W^{6+} ions substitute for Ta^{5+} ions in the perovskite BMT.

Scanning electron micrographs of the BMT-$x$$WO_3$ specimens ($x = 0.00, 0.02, 0.06$) are presented in Fig. 5. As indicated by arrows in Fig. 5c, minor phases are present in the 6 mol % WO_3-doped BMT. Both XRD (Fig. 4) and EPMA data suggest that the impurity phases are $Ba_{0.5}TaO_3$ and $BaWO_4$. On the other hand, a comparison of the scanning electron micrograph of the undoped BMT with that of the 2 mol % WO_3-doped BMT suggests that minor phases are absent in

Figure 6 Transmission electron micrograph (bright-field image) of BMT-0.02WO_3 sintered at 1600°C for 4hrs (×410,000).

the 2 mol % WO_3-doped BMT (Fig. 5a and b). Another evidence of the absence of impurity phases in the 2 mol % WO_3-doped BMT was obtained by examining the structure of intergranular region microscopically. As presented in Fig. 6, a typical bright-field image of the intergranular region also indicates the absence of minority phases in the 2 mol % WO_3-doped BMT. Therefore, one can conclude that the solubility limit of WO_3 in the perovskite BMT is approximately 2 mol %.

The apparent density of the BMT-$x$$WO_3$ specimens containing various amounts of WO_3 is presented in Fig. 7. As shown in the figure, the apparent density does not change up to 2 mol % WO_3 but decreases appreciably thereafter. One can attribute the observed decrease in the apparent density to the formation of low-density-phases. Since the theoretical density of the pure BMT is 7.637 g/cm^3 while those for $Ba_{0.5}TaO_3$ and $BaWO_4$

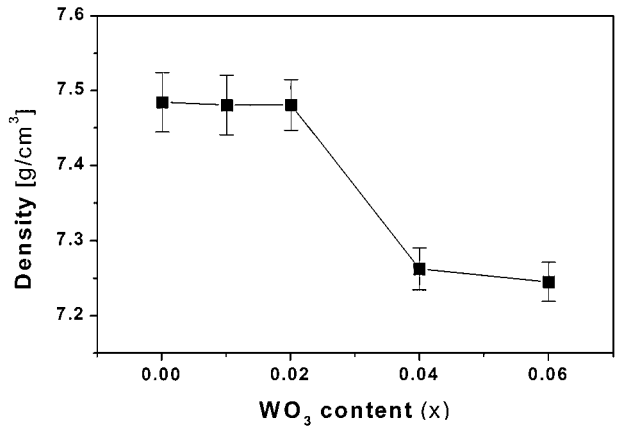

Figure 7 Apparent density of BMT-$x$$WO_3$ specimens containing various amounts of excess WO_3. The specimens were sintered at 1600°C for 4 hrs.

are 7.81 g/cm^3 and 6.382 g/cm^3, respectively [24], the result indicates the relative importance of the $BaWO_4$-formation above 2 mol %. Therefore, the estimated apparent density also suggests that the solubility limit of WO_3 in the BMT system is approximately 2 mol %, and this does accord with the result of XRD analysis (Fig. 4).

3.3. Defect mechanisms of $Ba(Mg_{1/3}Ta_{2/3})O_3$-based perovskites

The discussion made in the previous section concluded that W_{6+} ions substituted for Ta_{5+} ions in the WO_3-doped perovskite BMT. In this case, there exist two distinct defect chemical processes that satisfy the overall charge neutrality. They are (i) the liberation of electrons (electronic compensation) and (ii) the generation of tantalum and oxygen vacancies (ionic compensation). In this section, we will examine the main atomic defect mechanism associated with the dissolution of W-ions into the perovskite lattice. The elucidation of the charge compensation mechanism is important in the formation and growth of the long-range ordering because it is primarily responsible for the stabilization of the electrostatic repulsion arising from the formation of the positively charged $W^{\bullet}_{Ta}$ sites upon the substitution.

3.3.1. Defect mechanism of pure, undoped BMT

We will first examine the main intrinsic defect mechanism occurring in the pure, undoped BMT by analyzing the dependence of the electrical conductivity on the equilibrium partial pressure of oxygen. This analysis also gives us information on the nature of the charge carrier involved in BMT-based systems. In air atmosphere, one can consider the following dissolution/liberation equilibria of O_2 in the perovskite BMT:

$$1/2O_2 = 2/5V^{''''''}_{Ta} + O_O + 2h^{\bullet} \quad (3)$$

$$1/2O_2 = V''_{Ba} + O_O + 2h^{\bullet} \quad (4)$$

$$O_O = 1/2O_2 + V^{\bullet\bullet}_O + 2e' \quad (5)$$

where the defect reactions represented by Equations 3 and 4 are termed as oxidation, and Equation 5 as reduction. In addition to the above three reactions, one can also conceive the formation of magnesium vacancies (V''_{Mg}). In this case, a defect equation leading to oxidation is similar to Equation 4 because the ionic valence of magnesium is +2. However, considering the vapor pressure of the two constitutive metal oxides (vapor pressure of $MgO = 2.6 \times 10^{-3}$, 2.02×10^{-1}Pa and that of $BaO = 1.7 \times 10^{-2}$, 46.3 Pa at 1500 K and 2000 K, respectively) [25], one can expect that the vacancy formation at the Ba-sites (V''_{Ba}) dominates over the vacancy formation at the Mg-sites (V''_{Mg}). Therefore, we have relatively disregarded the formation of magnesium vacancies.

For a systematic discussion of the defect processes relevant to the present study, we have considered the mass-action relations. Equations 3–5 can be quantified by the following three mass-action relations, Equations 6–8, respectively:

$$K_{OX1} = \left[V^{''''''}_{Ta}\right]^{2/5} p^2 P_{O_2}^{-1/2} \quad (6)$$

$$K_{OX2} = \left[V^{''''''}_{Ba}\right] p^2 P_{O_2}^{-1/2} \quad (7)$$

$$K_{RED} = \left[V^{\bullet\bullet}_O\right] n^2 P_{O_2}^{1/2} \quad (8)$$

where [ ], n, and p, respectively, denote the concentrations of various vacancies, electrons, and holes, and K_{OX1}, K_{OX2}, and K_{RED} are the equilibrium constants for the oxidation process 1 (Equation 3), for the oxidation process 2 (Equation 4), and for the reduction (Equation 5), respectively. A fourth equation that satisfies the requirement of the electroneutrality can be written as

$$n + 2\left[V''_{Ba}\right] + 5\left[V^{''''''}_{Ta}\right] = p + 2\left[V^{\bullet\bullet}_O\right] \quad (9)$$

The above four equations allow us to estimate the concentrations of electrons or holes as a function of P_{O_2}. Using Equation 6 and the electroneutrality condition for Equation 3 (i.e., $5[V^{''''''}_{Ta}] = p$), the concentration of holes can be written as

$$p = \left\{5^{2/5} K_{OX1} P_{O_2}^{1/2}\right\}^{5/12} \propto P_{O_2}^{5/24} \quad (10)$$

Similarly, using Equation (7) and the electroneutrality condition for Equation 4 (i.e., $2[V''_{Ba}] = p$), the concentration of holes corresponding to Equation 4 can be written as

$$p = \left\{2K_{OX2} P_{O_2}^{1/2}\right\}^{1/3} \propto P_{O_2}^{1/6} \quad (11)$$

In the case of the reduction represented by Equation 5, the electroneutrality condition reads: $2[V^{\bullet\bullet}_O] = n$. Therefore, using Equation 8 one can readily obtain the following expression for the concentration of electrons:

$$n = \left\{2K_{RED} P_{O_2}^{-1/2}\right\}^{1/3} \propto P_{O_2}^{-1/6} \quad (12)$$

The main defect process occurring in the pure BMT can be identified by examining the electrical conductivity as a function of the partial pressure of oxygen, P_{O2}. The electrical conductivity data of the pure, undoped BMT specimen are shown in Fig. 8 as a function of P_{O2}. As indicated in the figure, the slope of $\log\sigma$ vs. $\log(P_{O2})$ plot is 1/6, indicating the importance of the oxidation reaction represented by Equation 4. Therefore, one can conclude that the major charge carriers of the undoped perovskite BMT are the holes produced by the oxidation and that the generation of holes is accompanied with the formation of barium vacancies.

3.3.2. Defect mechanism of WO_3-doped BMT

We are now in a position to elucidate the main defect process occurring in the presence of excess WO_3. As

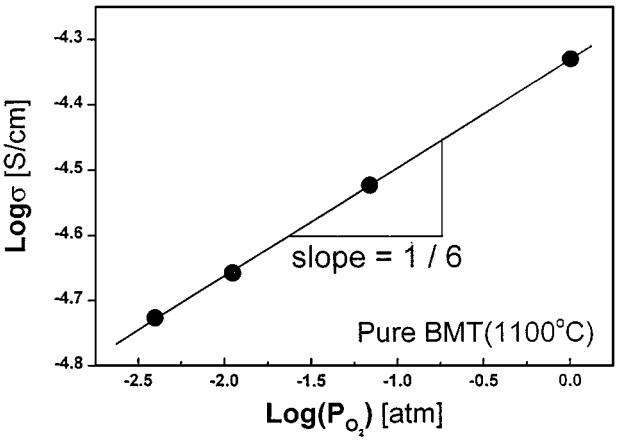

Figure 8 Electrical conductivity of undoped BMT specimen at 1100°C as a function of the partial pressure of oxygen.

discussed previously, the incorporation of excess WO_3 into the Ta-sites forming the positively charged $W_{Ta}^{\bullet}$ sites is accompanied either by the liberation of electrons or by the generation of $V_{Ta}^{''''''}$ and $V_O^{\bullet\bullet}$ vacancies via the following defect processes:

$$2WO_3 \overset{Ta_2O_5}{\longleftrightarrow} 2W_{Ta}^{\bullet} + 1/2O_2 + 5O_O + 2e' \quad (13)$$

$$WO_3 \overset{Ta_2O_5}{\longleftrightarrow} W_{Ta}^{\bullet} + V_{Ta}^{''''''} + 2V_O^{\bullet\bullet} + 3O_O \quad (14)$$

where the defect reaction represented by Equation 13 is termed as electronic compensation (EC) and the reaction described by Equation 14 as ionic compensation (IC). The atomic defect mechanism directly related to the dissolution of WO_3 can be identified by examining the electrical conductivity. Fig. 9 presents the reciprocal-temperature-dependence of logarithmic electrical conductivity for both the undoped BMT and the 2 mol % WO_3-doped BMT, measured by the 2-probe DC method. As shown in the figure, the electrical conductivity of the WO_3-doped BMT is consistently higher than that of the undoped BMT over a wide range of temperature.

We now examine the charge compensation mechanism occurring in the presence of excess WO_3. Let us

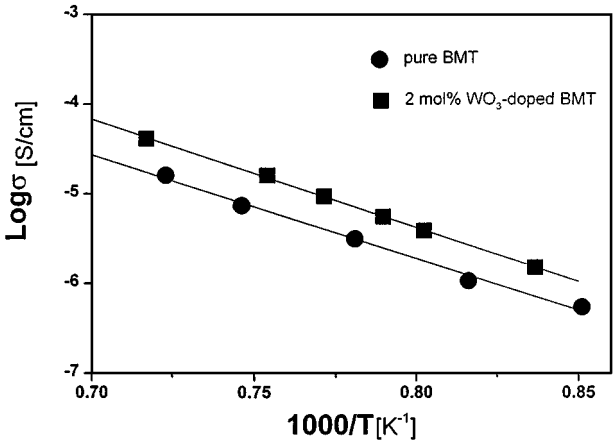

Figure 9 Reciprocal temperature dependence of logarithmic electrical conductivity of 2 mol % WO_3-doped BMT and undoped BMT specimens.

first suppose that the electronic compensation represented by Equation 13 is the main defect mechanism. Then, the incorporation of WO_3 into the Ta-sites would liberate electrons. Since the charge carrier of BMT-based specimens is hole, the electronic compensation mechanism then predicts a decrease in the electrical conductivity upon the substitution of W ions for Ta ions. However, the conductivity of the WO_3-doped BMT is higher than that of the undoped BMT for the whole range of temperature examined (Fig. 9). Therefore, the electronic compensation mechanism represented by Equation 13 is not relevant to the dissolution of WO_3 into the perovskite BMT and, thus, does not contribute significantly to the enhanced 1 : 2 ordering observed in the presence of WO_3 below the solubility limit.

Let us now assume that the ionic compensation described by Equation 14 is the main defect mechanism. Then, the positively charged mobile oxygen vacancies ($V_O^{\bullet\bullet}$) and the negatively charged tantalum vacancies ($V_{Ta}^{''''''}$) are simultaneously generated for the compensation of the positively charged $W_{Ta}^{\bullet}$ According to Equation 14, the concentration of oxygen vacancies should be twice as much as that of tantalum vacancies. Therefore, one can conclude that the increase in the electrical conductivity in the presence of WO_3 is mainly caused by the formation of oxygen vacancies. In addition to this, the activation energy of the 2 mol % WO_3-doped BMT was estimated to be about 1 eV. It was deduced from the σ-1/T diagram presented in Fig. 9. This value of the activation energy is nearly the same as that of other typical perovskite for the oxygen vacancy conduction: $\Delta E_{act} = 1.1$ eV for Al-doped $BaTiO_3$ [26]. Therefore, one can conclude that the addition of excess WO_3 to the perovskite BMT increases the electrical conductivity by generating the positively charged mobile vacancies($V_O^{\bullet\bullet}$) and that unfavorable repulsive electrostatic energy built in the 1 : 2 ordered domain by the formation of sites can be relieved by the ionic compensation mechanism, as described in Equation 14.

3.4. Effect of WO_3-content on the ordering and microchemistry

The TEM study (Fig. 1) indicated that, regardless of the WO_3-doping, only the long-range stoichiometric 1 : 2 ordering existed in the BMT-based perovskites. Fig. 10 presents the long-range order parameter of the stoichiometric 1 : 2 ordering in the BMT-$x$$WO_3$ specimens containing various amounts of WO_3. As shown in the figure, the estimated degree of the long-range ordering increases with the amount of excess WO_3 below the solubility limit (i.e., 2 mol %) while it decreases gradually thereafter.

It is well-known that the long-range cation ordering in A(B′, B″)O_3-type perovskites can be controlled not only by the heat treatment [8,9] but also by the concentration of vacancies [27–29]. For example, the degree of the B-site cation ordering in $Pb(Sc_{1/2}Ta_{1/2})O_3$ (PST) increases with increasing concentration of vacancy [27]. In addition to this, the local degree of ordering of a hot-pressed PST at near the grain boundary region having a higher vacancy concentration is higher than that

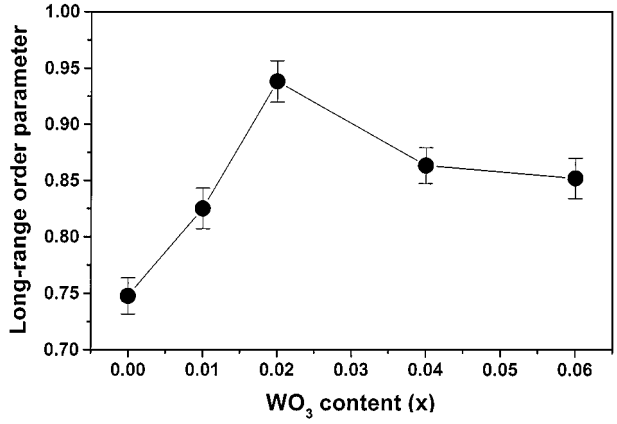

Figure 10 Long-range order parameter (S) of BMT-$x$$WO_3$ specimens plotted as a function of WO_3 content.

at the grain interior [29, 30]. Because the B-site cation ordering in A(B′, B″)O_3-type perovskites requires an atomic diffusion, these observations can be attributed to the enhanced diffusion rate caused by the increase in the concentration of vacancy.

As we have shown in the previous section, the WO_3-doping produces tantalum and oxygen vacancies below the solubility limit. Therefore, the enhanced diffusion rate of the B-site cations caused by the enhanced vacancy concentration seems to be mainly responsible for the observed increase in the long-range order parameter with the excess concentration of WO_3.

Finally, we will examine microchemical feature associated with the observed suppression of the 1 : 2 long-range ordering above the solubility limit of WO_3 (∼2 mol %). As discussed previously, both the XRD patterns (Fig. 4) and EPMA study indicated that Ba-containing second phases such as $Ba_{0.5}TaO_3$ and $BaWO_4$ were formed above the solubility limit of WO_3. For the formation of these phases, barium ions should first react with the excess-added WO_3 or the tantalum ions that are liberated by the dissolution of tungsten ions into the B-site sublattice. In addition to this, barium ions should also diffuse out from the interior perovskite grain. Since Ba^{2+} ion is significantly larger than the other two lattice-constitutive ions (effective ionic radius of $Ba^{2+} = 1.60$ Å, $Mg^{2+} = 0.72$ Å, and $Ta^{5+} = 0.64$ Å) [23], one can expect that the formation of second phases is more likely to initiate at a vacancy-rich region.

Because of the ionic charge compensation, the WO_3-doped grains contain more vacancies (V'''''_{Ta} and $V^{\bullet\bullet}_{O}$) than the undoped BMT grains, and this charge compensation mainly occurs within the 1 : 2 ordered region. Therefore, one does expect that an excessive doping of WO_3 expedites the formation of tantalum and oxygen vacancies above a certain critical concentration, thereby promoting the outer diffusion of Ba-ions from the perovskite lattice. This decreases the stability of the perovskite structure and, thus, suppresses the tendency of the long-range ordering, eventually leading to the collapse of the perovskite grain. Therefore, one can conclude that the observed decrease in the degree of the 1 : 2 long-range ordering above the solubility limit of WO_3 is directly related to the formation of second phases which is initiated by the excessive formation of tantalum and oxygen vacancies.

4. Conclusions

The nature of the long-range ordering in $Ba(B'_{1/3}B''_{2/3})O_3$-type perovskites was examined using the WO_3-doped $Ba(Mg_{1/3}Ta_{2/3})O_3$ as a model system. The following conclusions were made from the present study:

1. Regardless of the WO_3-doping, only the stoichiometric 1 : 2 long-range ordering of the B-site cation exists in the BMT-based perovskites.
2. The substitution of W^{6+} ions for Ta^{5+} ions in the B-site sublattice of the perovskite BMT produces the positively charged $W^{\bullet}_{Ta}$ sites with a concomitant generation of oxygen and tantalum vacancies for the ionic charge compensation. This ionic compensation mechanism relieves the electrostatic repulsion associated with the formation of the positively charged sites and, thus, eventually promotes the growth of the 1 : 2 long-range ordered domain.

Acknowledgement

This work was supported by "University Fundamental Research Fund, 1999" provided by the Ministry of Information and Communication (MIC) Republic of Korea.

References

1. M. FURUYA and A. OCHI, *Jpn. J. Appl. Phys.* **33** (1994) 5482.
2. T. S. RAO, V. R. K. MURTHY and B. VISWANATHAN, *Ferroelectrics* **102** (1990) 155.
3. K. WAKINO, *ibid.* **91** (1989) 69.
4. B. C. H. STEELE, "Electronic Ceramics" (Elsevier Applied Science, London and New York, 1991).
5. V. L. GUREVICH and A. K. TAGANTSEV, *Sov. Phys. JETP* **64** (1986) 142.
6. D. A. SAGALA and S. NAMBU, *J. Am. Ceram. Soc.* **75** (1992) 2573.
7. B. D. SILVERMAN, *Phys. Rev.* **125** (1962) 1921.
8. K. MATSUMOTO, T. HIUGA, K. TAKADA and H. ICHIMURA, in Proc. 6th IEEE Int. Symp. Appl. Ferroelectrics (1986) p. 118.
9. M. P. HARMER, J. CHEN, P. PENG, H. M. CHAN and D. M. SMYTH, *Ferroelectrics* **97** (1989) 263.
10. C. H. LU and C. C. TSAI, *J. Mater. Res.* **11** (1996) 1219.
11. X. M. CHEN, Y. SUZUKI and N. SATO, *J. Mater. Sci.* **5** (1994) 244.
12. S. NOMURA, *Ferroelectrics* **49** (1983) 61.
13. K. H. YOON, D. P. KIM and E. S. KIM, *J. Am. Ceram. Soc.* **77** (1994) 1062.
14. F. IZUMI, in "The Rietveld Method," edited by R. A. Young (Oxford University Press, New York, 1993) p. 236.
15. F. P. J. M. KERKHOF and J. A. MOULIJN, *J. Electron Spectroscopy and Related Phenomena* **14** (1978) 453.
16. D. A. SAGALA and S. NAMBU, *J. Phys. Soc. Jpn.* **61** (1992) 1791.
17. K.-M. LEE, H. M. JANG and W.-J. PARK, *J. Mater. Res.* **12** (1997) 1603.
18. K.-M. LEE and H. M. JANG, *J. Am. Ceram. Soc.* **81** (1998) 2586.
19. D. BRIGGS and M. P. SEAH, "Auger and X-ray Photoelectron Spectroscopy" (John Wiley and Sons, 1990).
20. R. J. COLTON and J. W. RABAIS, *Inorg. Chem.* **15** (1976) 236.
21. F. IZUMI, M. MITOMO and Y. BANDO, *J. Mater. Sci.* **19** (1984) 3115.
22. R. A. YOUNG and D. B. WILES, *J. Appl. Cryst.* **15** (1982) 435.

23. R. D. SHANNON and C. T. PREWITT, *Acta Cryst.* **B25** (1969) 925.
24. W. PIECE and A. WEISS, in "Landolt-Börnstein-Numerical Data and Functional Relationships in Science and Technology, New Series," edited by K. H. Helwege and A. M. Helwege (Springer-Verlag, 1973), Group III: Crystal and Solid State Physics. 7 [e].
25. G. V. SAMSONOV, "The Oxide Handbook" (IFI/PLENUM, 1982).
26. N.-H. CHAN, R. K. SHARMA and D. M. SMYTH, *J. Am. Ceram. Soc*. **65** (1982) 167.
27. I. M. REANEY, J. PETZELT, V. V. VOITSEKHOVSKII, F. CHU and N. SETTER, *J. Appl. Phys.* **76** (1994) 2086.
28. C. A. RANDALL, D. J. BARBER, R. W. WHATMORE and P. GROVES, *J. Mater. Sci*. **21** (1986) 4456.
29. G. KOSCHEK and E. KUBALEK, *J. Am. Ceram. Soc*. **68** (1985) 582.

Received 11 May 1999
and accepted 28 February 2000